Reduced anthropogenic aerosol radiative forcing caused by biogenic new particle formation

Hamish Gordon[a,1], Kamalika Sengupta[b], Alexandru Rap[b], Jonathan Duplissy[c], Carla Frege[d], Christina Williamson[e,f,g], Martin Heinritzi[e], Mario Simon[e], Chao Yan[h], João Almeida[a,e], Jasmin Tröstl[d], Tuomo Nieminen[c,i], Ismael K. Ortega[j,2], Robert Wagner[h], Eimear M. Dunne[b,k], Alexey Adamov[h], Antonio Amorim[l], Anne-Kathrin Bernhammer[m,n], Federico Bianchi[d,h], Martin Breitenlechner[m], Sophia Brilke[e], Xuemeng Chen[h], Jill S. Craven[o], Antonio Dias[a], Sebastian Ehrhart[a,e], Lukas Fischer[m], Richard C. Flagan[o], Alessandro Franchin[h], Claudia Fuchs[d], Roberto Guida[a], Jani Hakala[h], Christopher R. Hoyle[d,p], Tuija Jokinen[h], Heikki Junninen[h], Juha Kangasluoma[h], Jaeseok Kim[i,q], Jasper Kirkby[a,e], Manuel Krapf[d], Andreas Kürten[e], Ari Laaksonen[i,r], Katrianne Lehtipalo[d,h], Vladimir Makhmutov[s], Serge Mathot[a], Ugo Molteni[d], Sarah A. Monks[f,g], Antti Onnela[a], Otso Peräkylä[h], Felix Piel[e], Tuukka Petäjä[h], Arnaud P. Praplan[h], Kirsty J. Pringle[b], Nigel A. D. Richards[b,t], Matti P. Rissanen[h], Linda Rondo[e], Nina Sarnela[h], Siegfried Schobesberger[h], Catherine E. Scott[b], John H. Seinfeld[o], Sangeeta Sharma[t], Mikko Sipilä[c,h], Gerhard Steiner[h,m,u], Yuri Stozhkov[s], Frank Stratmann[u], Antonio Tomé[l], Annele Virtanen[i], Alexander Lucas Vogel[a], Andrea C. Wagner[e], Paul E. Wagner[u], Ernest Weingartner[d], Daniela Wimmer[h], Paul M. Winkler[u], Penglin Ye[v], Xuan Zhang[o], Armin Hansel[m,n], Josef Dommen[d], Neil M. Donahue[v], Douglas R. Worsnop[c,i,w], Urs Baltensperger[d], Markku Kulmala[c,h], Joachim Curtius[e], and Kenneth S. Carslaw[b,1]

[a]Department of Experimental Physics, CERN (European Organization for Nuclear Research), CH-1211 Geneva, Switzerland; [b]School of Earth and Environment, University of Leeds, Leeds LS2 9JT, United Kingdom; [c]Helsinki Institute of Physics, University of Helsinki, FI-00014 Helsinki, Finland; [d]Laboratory of Atmospheric Chemistry, Paul Scherrer Institute, CH-5232 Villigen, Switzerland; [e]Institute for Atmospheric and Environmental Sciences, Goethe University Frankfurt, 60438 Frankfurt am Main, Germany; [f]Cooperative Institute for Research in Environmental Sciences (CIRES), University of Colorado, Boulder, CO 80309; [g]Chemical Sciences Division, National Oceanic and Atmospheric Administration (NOAA) Earth System Research Laboratory, Boulder, CO 80305; [h]Department of Physics, University of Helsinki, FI-00014 Helsinki, Finland; [i]Department of Applied Physics, University of Eastern Finland, FI-70211 Kuopio, Finland; [j]Laboratoire de Physique des lasers, Atomes et Molcules Université Lille 1, UMR 8523 CNRS, 59655 Villeneuve d'Ascq, France; [k]Atmospheric Research Centre of Eastern Finland, Finnish Meteorological Institute, 70211 Kuopio, Finland; [l]Laboratory for Systems, Instrumentation and Modeling in Science and Technology for Space and the Environment, University of Lisbon and University of Beira Interior, 1849-016 Lisbon, Portugal; [m]Institute for Ion and Applied Physics, University of Innsbruck, 6020 Innsbruck, Austria; [n]Ionicon Analytik GmbH, 6020 Innsbruck, Austria; [o]Division of Chemistry and Chemical Engineering, California Institute of Technology, Pasadena, CA 91125; [p]Schnee- und Lawinenforschung (SLF), Eidgenössische Forschungsanstalt für Wald, Schnee und Landschaft (WSL) Institute for Snow and Avalanche Research, CH-7260 Davos, Switzerland; [q]Korea Polar Research Institute, 26 Songdomirae-ro, Yeonsu-gu, Incheon 21990, South Korea; [r]Climate Change Research Unit, Finnish Meteorological Institute, FI-00101 Helsinki, Finland; [s]Solar and Cosmic Ray Research Laboratory, Lebedev Physical Institute, 119991 Moscow, Russia; [t]National Centre for Earth Observation, University of Leeds, LS2 9JT Leeds, United Kingdom; [u]Faculty of Physics, University of Vienna, 1090 Vienna, Austria; [v]Center for Atmospheric Particle Studies, Carnegie Mellon University, Pittsburgh, PA 15213; and [w]Aerodyne Research Inc., Billerica, MA 01821

Edited by Joyce E. Penner, University of Michigan, Ann Arbor, MI, and accepted by Editorial Board Member A. R. Ravishankara August 20, 2016 (received for review February 19, 2016)

The magnitude of aerosol radiative forcing caused by anthropogenic emissions depends on the baseline state of the atmosphere under pristine preindustrial conditions. Measurements show that particle formation in atmospheric conditions can occur solely from biogenic vapors. Here, we evaluate the potential effect of this source of particles on preindustrial cloud condensation nuclei (CCN) concentrations and aerosol–cloud radiative forcing over the industrial period. Model simulations show that the pure biogenic particle formation mechanism has a much larger relative effect on CCN concentrations in the preindustrial atmosphere than in the present atmosphere because of the lower aerosol concentrations. Consequently, preindustrial cloud albedo is increased more than under present day conditions, and therefore the cooling forcing of anthropogenic aerosols is reduced. The mechanism increases CCN concentrations by 20–100% over a large fraction of the preindustrial lower atmosphere, and the magnitude of annual global mean radiative forcing caused by changes of cloud albedo since 1750 is reduced by 0.22 W m^{-2} (27%) to −0.60 W m^{-2}. Model uncertainties, relatively slow formation rates, and limited available ambient measurements make it difficult to establish the significance of a mechanism that has its dominant effect under preindustrial conditions. Our simulations predict more particle formation in the Amazon than is observed. However, the first observation of pure organic nucleation has now been reported for the free troposphere. Given the potentially significant effect on anthropogenic forcing, effort should be made to better understand such naturally driven aerosol processes.

aerosol | biogenic | forcing | climate

Measurements in the European Organization for Nuclear Research (CERN) Cosmics Leaving Outdoor Droplets (CLOUD) chamber under atmospheric conditions show that new particles can form purely from the oxidation products of α-pinene, a compound emitted by the biosphere (1). Nucleation of new aerosol particles via gas to particle conversion has been studied for 50 years (2) and is responsible for around one-half of global cloud condensation nuclei (CCN) (3), which affect Earth's radiation balance via aerosol–cloud interactions. The involvement of

Significance

A mechanism for the formation of atmospheric aerosols via the gas to particle conversion of highly oxidized organic molecules is found to be the dominant aerosol formation process in the preindustrial boundary layer over land. The inclusion of this process in a global aerosol model raises baseline preindustrial aerosol concentrations and could lead to a reduction of 27% in estimates of anthropogenic aerosol radiative forcing.

Author contributions: H.G., K.S., J. Kirkby, A.O., U.B., M. Kulmala, J.C., and K.S.C. designed research; H.G., K.S., A.R., J.A., J. Kirkby, S.A.M., K.J.P., N.A.D.R., C.E.S., S. Sharma, and K.S.C. performed research; H.G., K.S., J. Duplissy, C. Frege, C.W., M.H., M. Simon, C.Y., J.A., J.T., T.N., I.K.O., R.W., E.M.D., A. Adamov, A. Amorim, A.-K.B., F.B., M.B., S.B., X.C., J.S.C., A.D., S.E., L.F., R.C.F., A.F., C. Fuchs, R.G., J.H., C.R.H., T.J., H.J., J. Kangasluoma, J. Kim, J. Kirkby, M. Krapf, A.K., A.L., K.L., V.M., S.M., U.M., O.P., F.P., T.P., A.P.P., K.J.P., M.P.R., L.R., N.S., S. Schobesberger, J.H.S., S. Sharma, M. Sipilä, G.S., Y.S., F.S., A.T., A.V., A.L.V., A.C.W., P.E.W., E.W., D.R.W., P.M.W., P.Y., X.Z., A.H., J. Dommen, N.M.D., D.R.W., U.B., M. Kulmala, J.C., and K.S.C. collected data; and H.G., J. Kirkby, N.M.D., and K.S.C. wrote the paper.

The authors declare no conflict of interest.

This article is a PNAS Direct Submission. J.E.P. is a Guest Editor invited by the Editorial Board.

[1]To whom correspondence may be addressed. Email: hamish.gordon@cern.ch or k.s.carslaw@leeds.ac.uk.

[2]Present address: Office National d'Etudes et de Recherches Aérospatiales (ONERA), The French Aerospace Laboratory, F-91123 Palaiseau, France.

This article contains supporting information online at www.pnas.org/lookup/suppl/doi:10.1073/pnas.1602360113/-/DCSupplemental.

oxidized organic molecules in the process, alongside sulphuric acid, was proposed in early studies and has been well-established for some time (4, 5). The new mechanism for organic particle formation without sulphuric acid presented in ref. 1 could be important for Earth's climate, because it provides a way to form particles in the pristine preindustrial atmosphere, when the concentrations of sulphuric acid and ammonia were much lower. The preindustrial environment forms the baseline for calculations in global models of the radiative forcing caused by anthropogenic emissions (6), and uncertainties in this baseline are the largest component of the overall uncertainty on aerosol radiative forcing (7). The high sensitivity to the baseline is because an incremental increase in particle concentrations when they are low has a much stronger radiative effect than when they are high. Previous model uncertainty analyses suggested that the sensitivity of radiative forcing to particle formation rates is low compared with many other factors (7). However, these studies varied the nucleation rate assuming that sulphuric acid is required for particle production. Here, we show that the inclusion of a nucleation mechanism that does not require sulphuric acid could have a more significant effect on radiative forcing than previously thought (7, 8).

Our modeling study is inspired by and based on measurements in which α-pinene (AP), a volatile organic compound (VOC) emitted into the atmosphere by vegetation, was oxidized by ozone and hydroxyl radicals in the CLOUD chamber under ultraclean conditions without sulphuric acid (1). The mass spectra of the highly oxidized multifunctional organic molecules (HOMs) produced from the VOCs closely resemble those observed in the atmosphere (9). Therefore, although the concentrations of some reactive gases in the chamber do not perfectly match those in the troposphere, we have confidence in our assumption that the chamber results can be generalized to the atmosphere. Particle counters show that typical atmospheric concentrations of the HOMs produce particles at significant rates, even when sulphuric acid is absent from nucleating clusters. We describe this process as pure biogenic nucleation.

In this paper, we examine the implications of pure biogenic nucleation for atmospheric aerosol and Earth's radiative balance using the GLOMAP global model of aerosol microphysics (10). A parametrization of the pure biogenic nucleation rate that depends on the HOM concentration and the concentration of ions is provided in the supplementary materials in ref. 1. We assume for this study that this can be added linearly to parametrizations of the nucleation rate involving sulphuric acid only (11) and sulphuric acid with organics similar to HOMs (5). Ref. 1 also provided the yields of HOMs from the oxidation of AP by ozone (2.9%) and the hydroxyl radical (1.2%). The yield of HOMs from endocyclic monoterpenes, such as AP, is higher than that from exocylic monoterpenes, and therefore we separate these classes in our model and use the yields from β-pinene (BP) in ref. 12 to produce HOMs from exocylic monoterpenes. The rate of formation of 1.7-nm diameter aerosols by gas to particle conversion is, therefore, described by the sum of the following parametrizations.

i) Binary homogeneous nucleation of sulphuric acid and water (11).

ii) Nucleation of organics with sulphuric acid (5) also used in ref. 13:

$$J_{\mathrm{sa-org}} = k_{\mathrm{sa-org}}[\mathrm{H_2SO_4}]^2[\mathrm{BioOxOrg}], \quad [1]$$

where BioOxOrg refers to the oxidation products of monoterpenes with OH and $k_{\mathrm{sa-org}} = 3.27 \times 10^{-21}$ cm^6 s^{-1} (*Materials and Methods*).

iii) Pure biogenic nucleation, a sum of neutral (J_n) and ion-induced (J_{iin}) components (1):

$$J_{\mathrm{org}} = J_n + J_{iin}, \quad [2]$$

$$J_{\mathrm{n}} = a_1[\mathrm{HOM}]^{\frac{a_2+a_5}{[\mathrm{HOM}]}}, \quad [3]$$

and

$$J_{\mathrm{iin}} = 2[n_{\pm}]a_3[\mathrm{HOM}]^{\frac{a_4+a_5}{[\mathrm{HOM}]}}, \quad [4]$$

where HOMs are produced as described above but given here for convenience in units of 10^7 molecules per cubic centimeter, $n_{\pm}$ is the ion concentration, and a indicates free parameters. Ions in the model are produced from radon and galactic cosmic rays (*SI Appendix*).

Ammonia and amines can also contribute to nucleation by stabilizing sulphuric acid clusters, but the binary homogeneous mechanism has been shown to be a reasonable representation of free tropospheric nucleation (14), and nucleation at low altitudes involving amines or ammonia is important only in polluted regions, where the changes in radiative forcing calculated here are very insensitive to nucleation rates.

In our model, aerosols formed in this way and those emitted directly from Earth's surface grow by condensation and coagulation, are transported in the atmosphere, and are ultimately removed by dry or wet deposition. We consider the radiative forcing between 1750 and 2008 via the effect of these aerosols on cloud albedo, which is evaluated at the top of the atmosphere (0.03 Pa atmospheric pressure). To determine the effects of pure biogenic nucleation, particle formation rates, aerosol concentrations, and radiative forcing from model runs with and without mechanism *iii* are compared.

Biogenic Nucleation Rates and Observational Evidence

Fig. 1 shows the effect of pure biogenic nucleation on the preindustrial and present day atmospheres. When sulphuric acid is required for nucleation to proceed, substantially less nucleation is expected for preindustrial times (Fig. 1*A*) compared with the

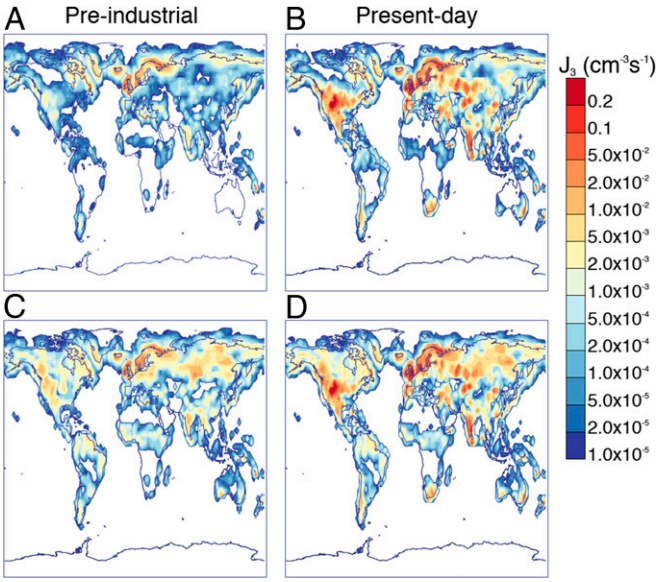

Fig. 1. Nucleation rates at 3-nm diameter (J_3, centimeters^{-3} second^{-1}) within approximately 500 m of the surface averaged over June without pure biogenic nucleation in (*A*) preindustrial and (*B*) present day conditions and with pure biogenic nucleation in (*C*) preindustrial and (*D*) present day conditions.

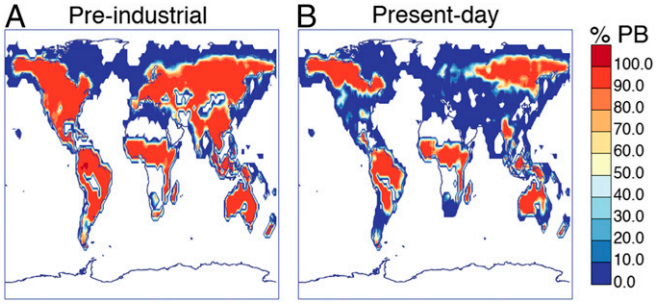

Fig. 2. Percentage of particles produced via pure biogenic (PB) nucleation within approximately 500 m of the surface averaged over June in (*A*) preindustrial and (*B*) present day conditions. We note that our model predicts large changes to particle formation at the surface and very little change above the boundary layer.

present day (Fig. 1*B*). However, when pure biogenic nucleation is included, the nucleation rates in preindustrial (Fig. 1*C*) and present-day times (Fig. 1*D*) become more similar. Although pure biogenic nucleation is much less important today (compare the change from Fig. 1*B* to Fig. 1*D* with that from Fig. 1*A* to Fig. 1*C*), it is still expected to be significant in some continental regions remote from pollution [for example, boreal regions, Australia, and according to our simulations (discussed later), the Amazon]. Within around 500 m of the surface, pure biogenic nucleation increases total production of particles of at least 3 nm in diameter via nucleation by 2.1% globally in the present day atmosphere but by 90% in preindustrial conditions.

Fig. 2 shows that pure biogenic nucleation is predicted to be the dominant mechanism for particle formation over large parts of the land surface above 50° N in summer even in the present day. However, both pure biogenic and sulphuric acid particle formation rates are often insufficient to produce detectable nucleation events (*SI Appendix*, Fig. S4). Pure biogenic nucleation has more effect in June than in January, because terpene emissions are higher in June. The diurnal cycles of nucleation rates at Hyytiälä and Pallas in Finland, shown in *SI Appendix*, Fig. S4, indicate that nucleation rates in these areas are occasionally higher than around 0.1 cm^{-3} s^{-1}. Experience from these boreal forest sites (15) suggests that nucleation rates above this value will result in detectable nucleation events. This approximate rule is confirmed by the modeled size distributions shown in *SI Appendix*, Fig. S6. As is observed, simulated nucleation rates are substantially higher during the day than at night.

To our knowledge, Hyytiälä and Jungfraujoch are the only locations with published measurements from the atmospheric pressure interface time-of-flight (APi-TOF) and chemical ionization-APi-TOF (CI-APi-TOF) mass spectrometers needed to unambiguously detect pure biogenic nucleation (15). There is strong evidence in ref. 16 that pure organic nucleation proceeds alongside sulphuric acid-driven nucleation at Jungfraujoch. For example, figure 2 in ref. 16 shows that, on the nucleation day 3, most organic clusters of masses of up to 400 amu contain no sulphuric acid, there is no inorganic nucleation, and the nucleation rate exceeds 10 cm^{-3} s^{-1} when sulphuric acid concentrations are less than 5×10^5 cm^{-3}.

There are no measurements of pure biogenic nucleation so far from Hyytiälä, because almost all of the nucleation rates measured in ref. 15 are at $[H_2SO_4] > 1 \times 10^6$ cm^{-3}. Observations at Hyytiälä were, however, used alongside those from Melpitz and Hohenpeissenberg to derive parametrizations of particle formation rates in ref. 17. The authors found that nucleation could be described well by

$$J_2 = k_1[H_2SO_4]^2 + k_2[H_2SO_4][org] + k_3[org]^2 \quad [5]$$

for constant k_{1-3}, suggesting that pure biogenic nucleation is a statistically detectable component of nucleation in these environments.

In addition to the Jungfraujoch observations, there is extensive circumstantial evidence for pure biogenic nucleation. The Amazon, where the lowest SO_2 concentrations over land are found, is an obvious place to look. Although some nucleation mode particles are seen in pristine regions of the Amazon (18) (on 19% of days sampled in the study referenced), no clear nucleation events or conclusive evidence for biogenic nucleation have yet been published, and growth of nucleation mode particles to CCN size is rarely observed there. Our model does not produce Hyytiälä-like nucleation events (*SI Appendix*, Figs. S5–S7), but it does predict nonzero particle formation rates. It slightly overestimates CCN concentrations compared with ref. 19 in the Amazon even without pure biogenic nucleation, and pure biogenic nucleation further increases the discrepancy by around a factor two. This discrepancy may point to a chemical suppression of HOM yields by isoprene (20) or NO_x (21) but could also be because of other sources of model error (for example, underestimation of particle size and therefore, condensation sink). Overprediction of particle concentrations over the Amazon seems to be a common feature among models (22). Comparing models with observations in this region is challenging because of large uncertainties in emissions of biogenic VOCs and a complex wet scavenging environment.

Pure biogenic nucleation is also predicted to be the dominant source of secondary particles in the cleanest high-latitude boreal regions. Low SO_2 concentrations, often below 100 ppt, and nocturnal nucleation were reported in a study at Värriö, Finland (67° N) at similar temperatures to the CLOUD chamber (23). Similar observations of nocturnal nucleation were made at Abisko, Sweden (24) and Tumbarumba, Australia (25), although SO_2 concentrations were not reported. At Pallas, Finland, H_2SO_4 concentrations are reported below 3×10^5 cm^{-3} in a large number of new particle formation events (26). The air masses in Pallas are usually of marine origin, which leads to low condensation sinks favorable to nucleation, but may also allow halogens of marine origin to locally influence nucleation. Three instances of new particle formation with $[H_2SO_4] < 3 \times 10^5$ cm^{-3} shown in figure 6 in ref. 26 are unambiguously continental, which should also allow the contribution of halogens to be excluded, making it highly likely the nucleation was pure biogenic.

With only sparse or indirect observational evidence for pure biogenic nucleation, an alternative strategy is to compare modeled particle concentrations against observations. However, this comparison is also inconclusive, because there are many compensating causes of model error (7), making attribution of biases ambiguous. Substantial changes in total particle number concentration are caused by pure biogenic nucleation (*SI Appendix*, Fig. S2). However, when we compare the monthly mean model predictions with particle number concentrations at 37 surface sites (27, 28) and the daily mean concentrations with those measured during the ARCTAS aircraft campaign (29) in 2008 (*SI Appendix*, Figs. S8 and S9), we find that the effect of pure biogenic mechanism, increasing summertime particle concentrations by up to a factor of two, is also comparable with or smaller than existing discrepancies between observations and the model.

Impact on CCN and Radiative Forcing

Fig. 3 shows the effect of pure biogenic nucleation on present day and preindustrial CCN concentrations calculated at 0.2% supersaturation. When pure biogenic nucleation is included, global annual average concentrations of these particles at cloud base level (approximately 600-m altitude) increase by 4% in the present day and 12% in the preindustrial atmospheres. Although nucleation rates are affected mostly close to sources of biogenic gases, CCN are affected over much wider areas because of the slower removal rate of larger aerosol particles. This spread is important, because it carries the particles to cloudy marine regions, where most of the anthropogenic aerosol–cloud radiative forcing occurs

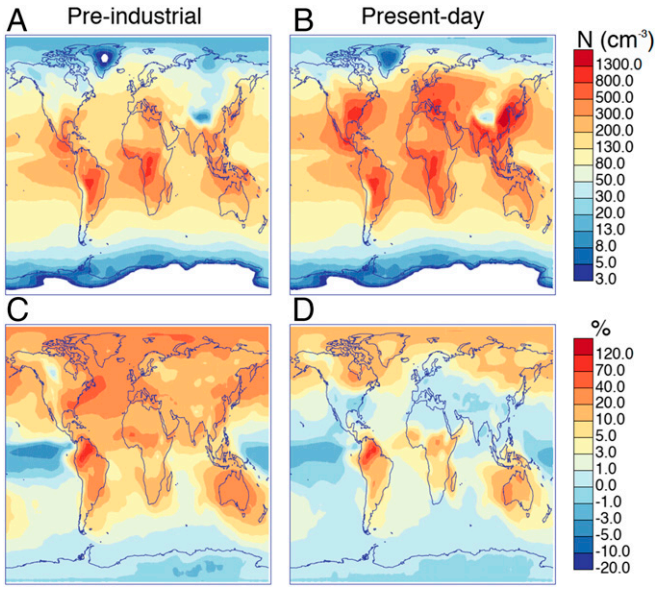

Fig. 3. Concentrations of CCN calculated at 0.2% supersaturation in centimeters^{-3} annually averaged at cloud base level in (*A*) preindustrial and (*B*) present day conditions, including pure biogenic nucleation and (*C* and *D*) percentage changes to these concentrations when pure biogenic nucleation is introduced. In this figure, we assume HOM formation and pure biogenic nucleation proceed at the rates measured at the CLOUD chamber.

(30). The change in CCN production across the pristine preindustrial atmosphere is particularly important for global climate, because cloud droplet concentrations and albedo are both more sensitive to CCN changes in pristine environments.

The effect of pure biogenic nucleation on the magnitude of aerosol radiative forcing from 1750 to 2008 was calculated by comparing simulations with and without pure biogenic nucleation. We only consider changes in the cloud albedo effect. The aerosol direct forcing is unlikely to be substantially influenced by the pure biogenic nucleation mechanism, because it is not strongly affected by the aerosol size distribution (31). The change in radiative forcing when pure biogenic nucleation is included is presented in Fig. 4. We estimate that the global annual mean cloud albedo forcing since 1750 after including pure biogenic nucleation is -0.60 W m^{-2}. The change in calculated aerosol radiative forcing caused by pure biogenic nucleation is $+0.22$ W m^{-2}, corresponding to a 27% reduction in the negative forcing. This change is a result of the nonlinear dependence of the forcing on the baseline CCN concentration (7). We note that our simulations may underestimate the net effect, because they do not account for possible increases in cloud fraction and thickness, which in pristine regions (CCN below 100 cm^{-3}), may be highly sensitive to small changes of CCN (32). We also do not account for the possibility of pure biogenic nucleation involving sesquiterpenes. However, we emphasize that including pure biogenic nucleation in our model leads to an overprediction of CCN in the Amazon region, which may indicate that it is chemically suppressed. Inhibition of nucleation, if it happens, may be local to the tropical rainforest environment or more widespread. If we artificially set pure biogenic nucleation rates to zero within 10° latitude of the equator, the change in aerosol forcing when pure biogenic nucleation is included changes only slightly to $+0.20$ W m^{-2}.

The largest changes in radiative forcing occur over the northern hemisphere (NH), especially over oceans with high annual cloud cover (Fig. 4*B*), where CCN concentrations are most strongly perturbed by anthropogenic emissions. The NH is also where pure biogenic nucleation causes the largest reduction in contrast between preindustrial and present day CCN concentrations driven by the large continental source of biogenic gases. However, the relative change in forcing in the southern hemisphere (SH) is greater than in the NH: pure biogenic nucleation reduces the annual southern hemispheric mean from -0.25 to -0.14 W m^{-2} (compared with a change in the NH from -1.39 to -1.06 W m^{-2}). In some tropical and southern regions, there are higher CCN concentrations in preindustrial times than today and a positive radiative forcing. In these regions and nearby, preindustrial OH· and HOMs were higher than today, and particle condensation sinks were lower, whereas SO_2 levels (largely marine) were comparable.

We consider the principal uncertainties in our analysis to be associated with (*i*) VOC, SO_2, and primary particle emissions such as in ref. 7); (*ii*) how representative AP and the pinanediol used in ref. 5 are of VOCs in the atmosphere; (*iii*) yields of HOMs from AP oxidation in the presence of other vapors, such as NO_x; and (*iv*) temperature dependence of the nucleation rates.

To investigate the effect of a plausible temperature dependence, we reran the model multiplying all boundary layer nucleation rates by $\exp(-(T-278)/10)$. The charged nucleation rate remained limited by the ion production rate and the overall rate by the kinetic limit. We find that annually averaged changes to cloud albedo radiative forcing over the industrial period from pure biogenic nucleation are reduced to $+0.14$ from $+0.22$ W m^{-2}.

The yields of HOMs have an experimental uncertainty around a factor of two [and were reported to be about a factor of two higher in an earlier chamber study (33)]. These uncertainties are comparable with uncertainties in the VOC emissions themselves (34). The yields could be affected by nitrogen oxides (21) and were found to differ

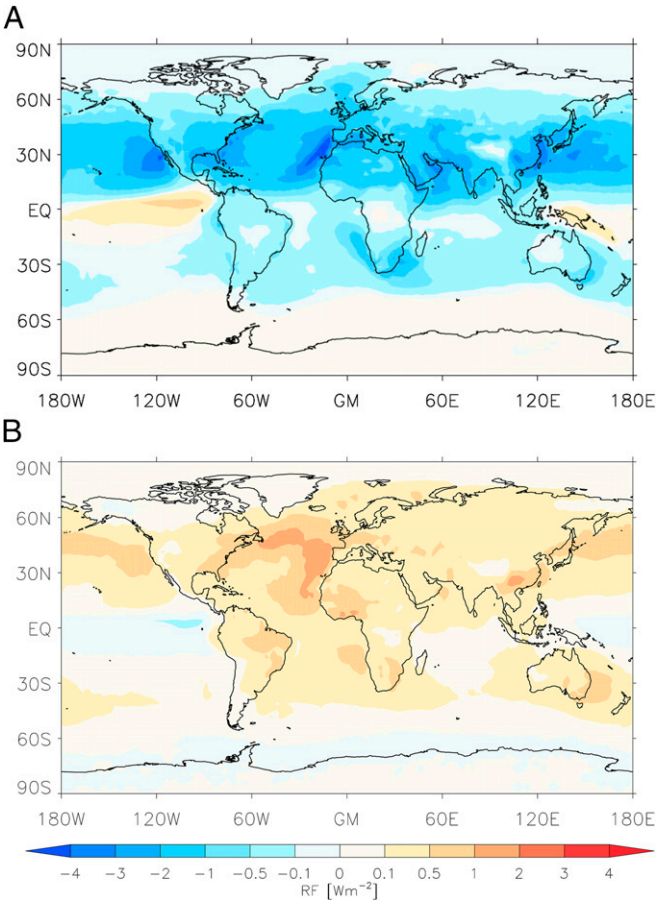

Fig. 4. (*A*) Distribution of cloud albedo radiative forcing, including pure biogenic nucleation and (*B*) change to this distribution when pure biogenic nucleation is included in the model. EQ, Equator; GM, Greenwich Meridian; RF, radiative forcing.

substantially between monoterpenes (12). To test the sensitivity to the uncertainty in yields, which is a proxy for the overall intrinsic uncertainty on the experimental measurements, we repeated our analysis with the yield of the HOMs that participate in pure biogenic nucleation perturbed by a factor of three. This perturbation gives an uncertainty range for the increase in CCN caused by the pure biogenic mechanism of 4 – 19% in preindustrial times and 1 – 6% in the present day as shown in *SI Appendix*, Table S2. The lower limit still leads to a significant change to cloud albedo forcing of 0.10 W m^{-2} when the corresponding parametrization is added to the model.

We have also investigated the sensitivity of our radiative forcing estimate to other sources of uncertainty. We perturb preindustrial volcanic SO_2 emissions and find that this does not strongly affect our reported CCN changes. When we perturb the biomass burning and sea spray emissions (details are in *SI Appendix*), we find larger changes to both CCN and forcing, especially when emissions are reduced. The model becomes slightly more sensitive to pure biogenic nucleation when a different baseline nucleation mechanism from ref. 17 instead of the one from ref. 5 is used. The percentage changes to CCN from including pure biogenic nucleation under these scenarios are given in *SI Appendix*, Table S2, and the changes to forcing are in *SI Appendix*, Table S3.

Discussion and Conclusions

Our global aerosol simulations indicate that pure biogenic nucleation (1) dominates particle formation in the preindustrial boundary layer, producing 59% of new particles below approximately 500-m altitude and 36% below around 1.5 km. For the organic system, laboratory measurements are currently the only route to a comprehensive understanding of the processes leading to particle formation. Laboratory measurements are especially valuable for a mechanism that is difficult to decouple from sulphuric acid-driven nucleation pathways in the polluted present day atmosphere. This mechanistic understanding is required to perform accurate extrapolations from present day conditions back to the preindustrial. Improving such extrapolations is of critical importance, because uncertainties in preindustrial aerosol are a large component of the uncertainty in Intergovernmental Panel on Climate Change (IPCC) estimates of radiative forcing. Although nucleation in tropical environments is relatively unimportant for global mean cloud albedo radiative forcing in our model, discrepancies between modeled and observed nucleation in these regions suggest that additional investigation of Amazon aerosol chemistry could significantly improve our understanding of pristine aerosol processes.

Based on the nucleation rates reported by CLOUD (1), we show here that pure biogenic nucleation may reduce the magnitude of preindustrial to present day aerosol cloud albedo forcing by as much as 0.22 W m^{-2} or 27%. This change in forcing is greater than the combined 1 standard deviation uncertainty of 28 parameters related to emissions and aerosol processes in this model (7), which is 19%. Other forcing mechanisms or uncertainties in the results quoted here could still lead to stronger effects. Although the calculated change in forcing is comparable with the model parametric uncertainty, it shifts the entire probability distribution of forcing, and therefore represents a significant downward revision in the likelihood of high negative aerosol–cloud forcings in this model. Similar revisions are likely to occur in other models (35) because of the same chain of processes: (*i*) proportionally greater increases in aerosol concentrations in the cleaner preindustrial atmosphere than in the present day, (*ii*) high sensitivity of cloud albedo and adjustments on the preindustrial aerosol concentrations, and (*iii*) reduction in the magnitude of anthropogenic aerosol radiative forcing by raising the preindustrial baseline aerosol concentration. To remain consistent with the observed temperature rise over the industrial period, reduced aerosol forcing implies reduced climate sensitivity (30, 36).

Materials and Methods

The modal version of the global aerosol model GLOMAP (10) is used to determine the impact of the biogenic nucleation mechanism reported in ref. 1. The model resolution is 2.8° × 2.8° horizontally, and there are 31 vertical levels from ground level to 10 hPa. GLOMAP is embedded within a chemical transport model, TOMCAT (37), and simulates the formation or emission, growth, coagulation, advection, cloud processing, and deposition of aerosol in seven log-normal size modes. Four modes (nucleation, Aitken, accumulation, and coarse) are hydrophilic, and there are also hydrophobic Aitken, accumulation, and coarse modes. The composition of each mode is determined by the relative fractions of the sulfate, sea salt, black carbon, and organic carbon compounds. Dust is not included, because it was not found to contribute significantly to CCN (38). Meteorology is forced by fields from the European Centre for Medium-Range Weather Forecasting. Total monoterpene emissions are taken from ref. 34, and the ratio of endocyclic to exocyclic monoterpenes was calculated from a run of the MEGAN model with the settings prescribed to follow ref. 39. Ref. 40 suggests that terpene emissions are (within uncertainties) unchanged through the industrial period.

Although sulphuric acid, ammonia, amines, halogens, and HOMs can all participate directly in nucleation, here we consider only sulphuric acid and HOMs. The HOMs are formed via the oxidation of monoterpenes by ozone (O_3) and hydroxyl radicals (OH·). The concentrations of these oxidants are read in every 6 h from a dedicated TOMCAT simulation. Instead of modeling the full reaction mechanism, we represent the HOM concentrations by

$$[\mathrm{HOM}] = \frac{(Y_{\mathrm{AP.O_3}} k_{\mathrm{AP.O_3}} [\mathrm{AP}][\mathrm{O_3}] + Y_{\mathrm{BP.O_3}} k_{\mathrm{BP.O_3}} [\mathrm{BP}][\mathrm{O_3}] + Y_{\mathrm{AP.OH\cdot}} k_{\mathrm{AP.OH\cdot}} [\mathrm{AP}][\mathrm{OH\cdot}] + Y_{\mathrm{BP.OH\cdot}} k_{\mathrm{BP.OH\cdot}} [\mathrm{BP}][\mathrm{OH\cdot}])}{CS},$$

where $Y_{\mathrm{AP.O_3}} = 2.9\%$ and $Y_{\mathrm{AP.OH\cdot}} = 1.2\%$ are the yields of HOMs from AP oxidation with ozone and hydroxyl radicals in the CLOUD chamber, respectively (described below), $Y_{\mathrm{BP.O_3}} = 0.12\%$ and $Y_{\mathrm{BP.OH\cdot}} = 0.58\%$ are taken from ref. 12, and *CS* is the condensation sink (seconds^{-1}) determined assuming the diffusion characteristics of a typical AP oxidation product (appendix A1 of ref. 10). The temperature-dependent reaction rate constant *k* values for oxidation of AP and BP by ozone and hydroxyl radicals are taken from the International Union of Pure and Applied Chemistry (IUPAC) (41).

The ozonolysis yield is determined with chemical ionization TOF mass spectrometers in the presence of a hydroxyl scavenger (0.1% H_2), replicating the effect of atmospheric OH· sinks, such as methane and carbon monoxide. The HOM yield from reaction with hydroxyl radicals is determined from measurements in the absence of ozone, where photolysed HONO provides the OH· source.

BioOxOrg in nucleation mechanism *ii* and HOMs in mechanism *iii* play equivalent roles, but the former refers to the parametrized oxidation products derived from pinanediol, a first generation oxidation product of AP. Its concentration, as described in ref. 5, is

$$[\mathrm{BioOxOrg}] = \frac{k_{\mathrm{AP.OH\cdot}} [\mathrm{AP}][\mathrm{OH\cdot}]}{CS},$$

where *CS* is the condensation sink. The BioOxOrg concentration was not measured directly in a mass spectrometer but calculated from the pinanediol concentration assuming a yield of 100%. The nucleation rate in mechanism *ii* is measured as a function of this BioOxOrg, and therefore, the yield is incorporated into the rate constant for nucleation. In ref. 5, monoterpenes are assumed to be equivalent to AP, and therefore, we assume only endocyclic monoterpenes participate in this nucleation mechanism.

Particles are formed according to the mechanisms described in the text at a critical diameter usually around 1.7 nm. Ion concentrations are determined by balancing production from radon and galactic cosmic rays with losses to preexisting particles and ion–ion recombination (*SI Appendix*). The formation rates are then adjusted to account for losses during the initial growth with the Kerminen–Kulmala equation (42) using growth rates taken from the parametrization of ref. 43.

Particles subsequently grow by kinetic condensation of organic molecules produced from oxidation of terpenes or isoprene by nitrate or hydroxyl radicals or by ozone, with a 13% assumed yield for terpenes (10) and a 3% yield for isoprene (44). They also coagulate, and hence, the overall particle number is determined by solving the coagulation–nucleation equation (10). Finally, particles may be lost by dry or wet deposition.

Present day simulations are run for 2008, and preindustrial simulations are run with 2008 meteorology and 1750 emissions. For the 1750 simulation, anthropogenic sources of SO_2 and H_2SO_4 were removed from the model, OH, NO_3, and ozone concentrations were adjusted to preindustrial levels determined from a dedicated TOMCAT simulation, and black and organic carbon primary emissions were adjusted to a representation of preindustrial levels.

CCN and cloud droplet number concentrations (CDNCs) are calculated for each simulation from the particle size distributions using the parametrization of ref. 45, assuming for the CDNCs constant updraft velocities of 0.15 ms^{-1} over sea and 0.30 ms^{-1} over land. The hygroscopicity parameters assigned to each chemical component follow ref. 44: sulfate (0.61; assuming ammonium sulfate), sea salt (1.28), black carbon (0.0), and organics (0.1). The change in cloud droplet effective radii corresponding to the CDNC change is calculated in accordance with ref. 31, whereas the cloud albedo is estimated using the radiative transfer model of ref. 46.

ACKNOWLEDGMENTS. We thank P. Carrie, L.-P. De Menezes, J. Dumollard, F. Josa, I. Krasin, R. Kristic, A. Laassiri, O. S. Maksumov, B. Marichy, H. Martinati, S. V. Mizin, R. Sitals, A. Wasem, and M. Wilhelmsson for their important contributions to the experiment. We also thank D. Veber from Environment and Climate Change Canada for maintenance and calibrations of instruments at East Trout Lake and the Earth System Research Laboratory of the National Oceanic and Atmospheric Administration for collaboration with data collection and quality assurance and control software. We thank A. D. Clarke and C. L. S. Reddington for making available processed data from the Arctic Research of the Composition of the Troposphere from Aircraft and Satellites (ARCTAS) campaign. We thank the European Organization for Nuclear Research (CERN) for supporting CLOUD with important technical and financial resources and providing a particle beam from the CERN Proton Synchrotron. The global modelling simulations were performed on Advanced Research Computing (ARC) high-performance computers at the University of Leeds. This research has received funding from the European Commission (EC) Seventh Framework and Horizon 2020 Programmes [Marie Curie Initial Training Network (MC-ITN) CLOUD-TRAIN Grant 316662, Marie Sklodowska-Curie Grants 656994 and 600377, European Research Council (ERC)-Consolidator Grant NANODYNAMITE 616075, and ERC-Advanced Grant ATMNUCLE 227463]; German Federal Ministry of Education and Research Project 01LK1222A; Swiss National Science Foundation Projects 200020_135307, 200021_140663, 206021_144947/1, and 20FI20_149002/1; Academy of Finland Center of Excellence Project 1118615; Academy of Finland Grants 135054, 133872, 251427, 139656, 139995, 137749, 141217, and 141451; the Finnish Funding Agency for Technology and Innovation; the Väisälä Foundation; the Nessling Foundation; Austrian Science Fund Project L593; Portuguese Foundation for Science and Technology Project CERN/FP/116387/2010; Swedish Research Council, Vetenskapsrådet Grant 2011-5120; Presidium of the Russian Academy of Sciences and Russian Foundation for Basic Research Grant 12-02-91522-CERN; United Kingdom Natural Environment Research Council Grant NE/K015966/1; the Royal Society (Wolfson Merit Award); National Science Foundation Grants AGS1136479, AGS1439551, AGS1447056, and CHE1012293; Caltech Environmental Science and Engineering Grant (Davidow Foundation); Dreyfus Award EP-11-117; the French National Research Agency; the Nord-Pas de Calais; and European Funds for Regional Economic Development Labex-Cappa Grant ANR-11-LABX-0005-01.

1. Kirkby J, et al. (2016) Ion-induced nucleation of pure biogenic particles. *Nature* 533(7604):521–526.
2. Went FW (1960) Blue hazes in the atmosphere. *Nature* 187(4738):641–643.
3. Merikanto J, Spracklen DV, Mann GW, Pickering SJ, Carslaw KS (2009) Impact of nucleation on global CCN. *Atmos Chem Phys* 9(21):8601–8616.
4. Kavouras IG, Mihalopoulos N, Stephanou EG (1998) Formation of atmospheric particles from organic acids produced by forests. *Nature* 395(6703):683–686.
5. Riccobono F, et al. (2014) Oxidation products of biogenic emissions contribute to nucleation of atmospheric particles. *Science* 344(6185):717–721.
6. Hansen J, et al. (1981) Climate impact of increasing atmospheric carbon dioxide. *Science* 213(4511):957–966.
7. Carslaw KS, et al. (2013) Large contribution of natural aerosols to uncertainty in indirect forcing. *Nature* 503(7474):67–71.
8. Pierce JR, Adams PJ (2009) Uncertainty in global CCN concentrations from uncertain aerosol nucleation and primary emission rates. *Atmos Chem Phys* 9(4):1339–1356.
9. Schobesberger S, et al. (2013) Molecular understanding of atmospheric particle formation from sulfuric acid and large oxidized organic molecules. *Proc Natl Acad Sci USA* 110(43):17223–17228.
10. Mann GW, et al. (2010) Description and evaluation of GLOMAP-mode: A modal global aerosol microphysics model for the UKCA composition-climate model. *Geosci Model Dev* 3(2):519–551.
11. Vehkamäki H, et al. (2002) An improved parameterization for sulfuric acid-water nucleation rates for tropospheric and stratospheric conditions. *J Geophys Res* 107(D22): 4622.
12. Jokinen T, et al. (2015) Production of extremely low volatile organic compounds from biogenic emissions: Measured yields and atmospheric implications. *Proc Natl Acad Sci USA* 112(23):7123–7128.
13. Yu F, et al. (2015) Spring and summer contrast in new particle formation over nine forest areas in North America. *Atmos Chem Phys* 15(24):13993–14003.
14. Spracklen DV, Pringle KJ, Carslaw KS, Chipperfield MP, Mann GW (2005) A global off-line model of size-resolved aerosol microphysics. II. Identification of key uncertainties. *Atmos Chem Phys* 5(12):3233–3250.
15. Kulmala M, et al. (2013) Direct observations of atmospheric aerosol nucleation. *Science* 339(6122):943–946.
16. Bianchi F, et al. (2016) New particle formation in the free troposphere: A question of chemistry and timing. *Science* 352(6289):1109–1112.
17. Paasonen P, et al. (2010) On the roles of sulphuric acid and low-volatility organic vapours in the initial steps of atmospheric new particle formation. *Atmos Chem Phys* 10(22):11223–11242.
18. Rizzo L, Artaxo P, Karl T, Guenther A, Greenberg J (2010) Aerosol properties, in-canopy gradients, turbulent fluxes and VOC concentrations at a pristine forest site in Amazonia. *Atmos Environ* 44(4):503–511.
19. Martin S, et al. (2010) Sources and properties of Amazonian aerosol particles. *Rev Geophys* 48:RG2002.
20. Kiendler-Scharr A, et al. (2009) New particle formation in forests inhibited by isoprene emissions. *Nature* 461(7262):381–384.
21. Wildt J, et al. (2014) Suppression of new particle formation from monoterpene oxidation by NO_x. *Atmos Chem Phys* 14(6):2789–2804.
22. Mann GW, et al. (2014) Intercomparison and evaluation of global aerosol microphysical properties among AeroCom models of a range of complexity. *Atmos Chem Phys* 14(9):4679–4713.
23. Vehkamäki H, et al. (2004) Atmospheric particle formation events at Värriö measurement station in Finnish Lapland 1998-2002. *Atmos Chem Phys* 4(7):2015–2023.
24. Svenningsson B, et al. (2008) Aerosol particle formation events and analysis of high growth rates observed above a subarctic wetland–forest mosaic. *Tellus B Chem Phys Meterol* 60(3):353–364.
25. Suni T, et al. (2008) Formation and characteristics of ions and charged aerosol particles in a native Australian Eucalypt forest. *Atmos Chem Phys* 8(1):129–139.
26. Asmi E, et al. (2011) Secondary new particle formation in Northern Finland Pallas site between the years 2000 and 2010. *Atmos Chem Phys* 11(24):12959–12972.
27. Spracklen DV, et al. (2010) Explaining global surface aerosol number concentrations in terms of primary emissions and particle formation. *Atmos Chem Phys* 10:4775–4793.
28. Torseth K, et al. (2012) Introduction to the European Monitoring and Evaluation Programme (EMEP) and observed atmospheric composition change during 1972-2009. *Atmos Chem Phys* 12:5447–5481.
29. Jacob DJ, et al. (2010) The Arctic Research of the Composition of the Troposphere from Aircraft and Satellites (ARCTAS) mission: Design, execution, and first results. *Atmos Chem Phys* 10(11):5191–5212.
30. Charlson RJ, et al. (1992) Climate forcing by anthropogenic aerosols. *Science* 255(5043):423–430.
31. Rap A, et al. (2013) Natural aerosol direct and indirect radiative effects. *Geophys Res Lett* 40(12):3297–3301.
32. Koren I, Dagan G, Altaratz O (2014) From aerosol-limited to invigoration of warm convective clouds. *Science* 344(6188):1143–1146.
33. Ehn M, et al. (2014) A large source of low-volatility secondary organic aerosol. *Nature* 506(7489):476–479.
34. Sindelarova K, et al. (2014) Global data set of biogenic VOC emissions calculated by the MEGAN model over the last 30 years. *Atmos Chem Phys* 14(17):9317–9341.
35. Myhre G, et al. (2013) Radiative forcing of the direct aerosol effect from AeroCom Phase II simulations. *Atmos Chem Phys* 13(4):1853–1877.
36. Knutti R, Stocker TF, Joos F, Plattner G-K (2002) Constraints on radiative forcing and future climate change from observations and climate model ensembles. *Nature* 416(6882):719–723.
37. Chipperfield MP (2006) New version of the TOMCAT/SLIMCAT off-line chemical transport model: Intercomparison of stratospheric tracer experiments. *Q J R Meteorol Soc* 132(617):1179–1203.
38. Manktelow PT, Carslaw KS, Mann GW, Spracklen DV (2010) The impact of dust on sulfate aerosol, CN and CCN during an East Asian dust storm. *Atmos Chem Phys* 10(2):365–382.
39. Guenther A, et al. (2012) The Model of Emissions of Gases and Aerosols from Nature version 2.1 (MEGAN2.1): An extended and updated framework for modeling biogenic emissions. *Geosci Model Dev* 5(6):1471–1492.
40. Acosta Navarro JC, et al. (2014) Global emissions of terpenoid VOCs from terrestrial vegetation in the last millennium. *J Geophys Res Atmos* 119(11):6867–6885.
41. Atkinson R, et al. (2006) Evaluated kinetic and photochemical data for atmospheric chemistry: Volume II: Gas phase reactions of organic species. *Atmos Chem Phys* 6(11): 3625–4055.
42. Kerminen V-M, Kulmala M (2002) Analytical formulae connecting the real and the apparent nucleation rate and the nuclei number concentration for atmospheric nucleation events. *J Aerosol Sci* 33(4):609–622.
43. Tröstl J, et al. (2016) The role of low-volatility organic compounds in initial particle growth in the atmosphere. *Nature* 533(7604):527–531.
44. Scott CE, et al. (2014) The direct and indirect radiative effects of biogenic secondary organic aerosol. *Atmos Chem Phys* 14(1):447–470.
45. Morales R, Nenes A, Jonsson H, Flagan RC, Seinfeld JH (2011) Evaluation of an entraining droplet activation parameterization using in situ cloud data. *J Geophys Res Atmos* 116:D15205.
46. Edwards JM, Slingo A (1996) Studies with a flexible new radiation code. I. Choosing a configuration for a large-scale model. *Q J R Meteorol Soc* 122(531):689–719.